5644 *Chem. Mater.* **2009,** *21,* 5644–5653
DOI:10.1021/cm902854d

CHEMISTRY OF MATERIALS
Article

Block Copolymer-Mediated Formation of Superparamagnetic Nanocomposites

Sanchita Biswas,[†] Kevin D. Belfield,*[,†] Ritesh K. Das[‡] Siddhartha Ghosh,[‡] and Arthur F. Hebard[‡]

[†]*Department of Chemistry, University of Central Florida, P.O. Box 162366, Orlando, Florida 32816-2366 and* [‡]*Department of Physics, University of Florida, Gainesville, Florida 32611*

Received September 11, 2009. Revised Manuscript Received October 28, 2009

Well-defined diblock copolymers of bicyclo[2.2.1]hept-5-ene-2-carboxylic acid oxiranylmethyl ester, having both anchoring and steric stabilizing blocks in a 1:1 ratio, have been prepared by ring-opening metathesis polymerization (ROMP). The epoxy-containing block copolymer stabilized in situ generated iron oxide (γ-Fe_2O_3) nanoparticles. The epoxy ester group provided strong chelation between the iron-oxide nanoparticle and the polymeric siderophores, producing a stable magnetic nanocomposite. The polymers were characterized by ^{1}H NMR, GPC, TGA, and DSC. The morphology and crystalline structure of the maghemite−block copolymer nanocomposites were evaluated with TEM and XRD, revealing highly crystalline, monodisperse γ-Fe_2O_3 nanoparticles with an average size of 3−5 nm. Interactions between the maghemite nanoparticles and the polymer were observed by FTIR. SQUID magnetometric analysis of the nanocomposites demonstrated superparamagnetism at room temperature with high saturation magnetization.

Introduction

Nanoparticles embedded in self-assembled block copolymers have generated interest as a tool in a number of applications due to several advantageous properties obtained from the combination of organic polymers and inorganic metal/metal oxide nanoparticles.[1−4] Among the various magnetic nanoparticles, magnetic metal oxide nanoparticles, particularly maghemite and magnetite, have attracted attention due to their large ratio of surface area to volume, high magnetization, low magnetic remanence and coercivity, and low toxicity. Maghemite nanoparticles with diameters ranging from 1 to 10 nm exhibit superparamagnetism at room temperature and have applications in ferrofluids[5] and biomedical imaging. The most significant applications of magnetic nanoparticles in the biomedical imaging field are as negative contrast agents in magnetic resonance imaging (MRI),[6−8] non-invasive local drug and gene delivery,[9] clinical diagnosis,[10] bioseparations of DNA,[11] cell surface receptor targeting,[12] and treatment of hyperthermia.[13] Superparamagnetic nanoparticles are promising for a variety of biomimetic engineering applications, including magnetosomes,[14] nanobots,[15] and artificial muscles.[16−18] The important criteria for biomimetic applications are high instantaneous magnetization in the presence of an external magnetic field, complete removal of magnetic properties in the absence of a magnetic field, small particle size, and strong interactions between magnetic nanoparticles and the dispersing media so that all move together under magnetic stimulation without sacrificing stability.[16]

A major, fundamental problem of nanoscale maghemite particles is aggregation and cluster formation that eventually nullifies the benefits related to their

(1) Balazs, A. C.; Emrick, T.; Russell, T. P. *Science* **2006**, *314*, 1107–1110.
(2) Pyun, J. *Polym. Rev.* **2007**, *47*, 231–263.
(3) Sanchez, C.; Julián, B.; Belleville, P.; Popall, M. *J. Mater. Chem.* **2005**, *15*, 3559–3592.
(4) Sun, S.; Anders, S.; Hamann, H. F.; Thiele, J. U.; Baglin, J. E. E.; Thomson, T.; Fullerton, E. E.; Murray, C. B.; Terris, B. D. *J. Am. Chem. Soc.* **2002**, *124*, 2884–2885.
(5) Mornet, S.; Portier, J.; Duguet, E. *J. Magn. Magn. Mater.* **2005**, *293*, 127–134.
(6) Martina, M. S.; Fortin, J. P.; Menager, C.; Clement, O.; Barratt, G.; Grabielle-Madelmont, C.; Gazeau, F.; Cabuil, V.; Lesieur, S. *J. Am. Chem. Soc.* **2005**, *127*, 10676–10685.
(7) Berret, J. F.; Schonbeck, N.; Gazeau, F.; El Kharrat, D.; Sandre, O.; Vacher, A.; Airiaus, M. *J. Am. Chem. Soc.* **2006**, *128*, 1755–1761.
(8) Lutz, J. F.; Stiller, S.; Hoth, A.; Kaufner, L.; Pison, U.; Cartier, R. *Biomacromolecules* **2006**, *7*, 3132.
(9) Tanaka, T.; Sakai, R.; Kobayashi, R.; Hatakeyama, K.; Matsunaga, T. *Langmuir* **2009**, *25*, 2956–2961.
(10) Perez, J. M.; Josephson, L.; Weissleder, R. *Chembiochem* **2004**, *5*, 261–264.
(11) Boyer, C.; Bulmus, V.; Teoh, W. Y.; Amal, R.; Davis, T. P. *J. Mater. Chem.* **2009**, *19*, 111–123.
(12) Shukoor, M. I.; Natalio, F.; Metz, N.; Glube, N.; Tahir, M. N.; Therese, H. A.; Ksenofontov, V.; Theato, P.; Langguth, P.; Boissel, J. P. *Angew. Chem., Int. Ed.* **2008**, *47*, 4748–4752.
(13) Sonvico, F.; Mornet, S.; Vasseur, S.; Dubernet, C.; Jaillard, D.; Degrouard, J.; Hoebeke, J.; Duguet, E.; Colombo, P.; Couvreur, P. *Bioconjugate Chem.* **2005**, *16*, 1181–1188.
(14) Lang, C.; Schueler, D.; Faivre, D. *Macromol. Biosci.* **2007**, *7*, 144–151.
(15) Sitti, M. *Nature* **2009**, *458*, 1121–2.
(16) Albornoz, C.; Jacobo, S. E. *J. Magn. Magn. Mater.* **2006**, *305*, 12–15.
(17) Shin, M. K.; Kim, S. I.; Kim, S. J.; Park, S. Y.; Hyun, Y. H.; Lee, Y. P.; Lee, K. E.; Han, S. S.; Jang, D. P.; Kim, Y. B. *Langmuir* **2008**, *24*, 12107–12111.
(18) Chuang, C. J.; Li, W. S.; Lai, C. C.; Liu, Y. H.; Peng, S. M.; Chao, I.; Chiu, S. H. *Org. Lett.* **2008**, *11*, 385–388.

Published on Web 11/11/2009

nanoscopic dimensions. There is strong theoretical as well as experimental support that the morphology and behavior of the nanocomposites can be modulated by tailoring the ligands of well-defined, functional polymers, depending on the size of the nanoparticles.[19,20] The magnetic core with polymeric shell-type structures isolate and disperse magnetic nanoparticles by the interaction of nanoparticles and polymers, mediated through ligands attached to the surface of the polymers. Ligands attached to the polymer matrix not only prevent the agglomeration of the nanoparticles but also provide a tool to tune the magnetic properties of the system. Commonly used ligands for magnetic nanoparticle (NP) stabilization include carboxyl,[21−23] hydroxy,[9,24] amine[25] or imine,[26−28] phosphine oxides,[29] and phosphonic acid.[11] Ligands markedly influence the particle's spatial behavior as well as ultimate macroscopic properties of the polymer−nanocomposites. However, more efforts are needed in the design and synthesis of more efficient stabilizers for monodispersed maghemite nanocomposites with sufficient intrinsic magnetization and versatile surface functionality.[30] Currently, the synthesis of well-defined nanocomposites in self-assembled structures, such as polymers or surfactants, has become simpler and more efficient relative to other complex processes, such as biomineralization.[22,31−34] Diblock copolymer templates containing both steric stabilizing groups and anchoring ligands, to prevent the aggregation of the NPs offers microphase separation of the copolymer, thus controling the spatial distribution and inherent properties of the nanocomposites.

Ring-opening metathesis polymerization (ROMP) is a well established tool in order to synthesize well-defined, highly functionalized block copolymers.[35,36] The energetics of strained bicyclic olefin monomers is thermodynamically favorable to yield stereoregular and monodispersed polymers.[37] The polymerization process is also dependent on a number of physical factors such as monomer concentration, temperature, pressure, and the chemical nature and position of substituents on the ring. Over the past decade, Grubbs' ruthenium-based catalysts have shown a broad range of functionalization due to their high tolerance of heteroatom-containing groups which had poisoned earlier catalysts.[32]

Herein, we demonstrate a strategy for the synthesis of well-defined diblock copolymers with a norbornene-based backbone, using ROMP. The copolymers contain "iron-loving" siderophores in one block to chelate and interact with iron oxide nanoparticle surfaces and a steric stabilizing group in the other block to prevent metal nanopartcle aggregation. The siderophores are designed with the following versatility: (1) use of epoxide/oxirane anchoring group to stabilize the maghemite nanoparticles while retaining supermagnetic properties and (2) further flexibility of design by reaction of the oxirane group to modify the ligand via, e.g., nucleophilic reaction or hydrolysis.[38−42] This leads to straghtforward formation of maghemite−diblock copolymer nanocomposites and construction of a broad range of functionalities on the periphery of the block copolymers to stabilize the nanoparticles. Norbornene-based polymers have a number of interesting properties such as high thermal stability, optical transparency, and a low dielectric constant with a generally amorphous morphology. We report strategies to synthesize epoxy-containing diblock copolymers via ROMP that are well-characterized by NMR, elemental analysis, gel permeation chromatography (GPC), thermogravimetric analysis (TGA), and differential scanning calorimetry (DSC). The polymer−maghemite nanocomposites with different polymer nanoparticle formulations were prepared through a nonhydrolytic method in the polymer microdomains with nanoparticle sizes ranging between 2 and 6 nm. The polymer composites were characterized by transmission electron microscopy (TEM), Fourier transform infrared spectroscopy (FTIR), and X-ray diffraction (XRD) in order to elucidate the nanoparticle size, nanoparticle−ligand interactions, and nanoparticle crystalline morphology, respectively. Magnetic properties of the nanocomposites were determined using superconducting quantum interference device (SQUID) through measuring magnetization as a function of temperature or applied magnetic field and establishing the superparamagnetism properties at room temperature.

(19) Thompson, R. B.; Ginzburg, V. V.; Matsen, M. W.; Balazs, A. C. *Science* **2001**, *292*, 2469–2472.
(20) Kim, J. U.; O; Shaughnessy, B. *Macromolecules* **2006**, *39*, 413–425.
(21) Harris, L. A.; Goff, J. D.; Carmichael, A. Y.; Riffle, J. S.; Harburn, J. J.; Pierre, T. G. S.; Saunders, M. *Chem. Mater*. **2003**, *15*, 1367–1377.
(22) Sohn, B. H.; Cohen, R. E. *Chem. Mater*. **1997**, *9*, 264–269.
(23) Wu, C. K.; Hultman, K. L.; O'Brien, S.; Koberstein, J. T. *J. Am. Chem. Soc*. **2008**, *130*, 3516–3520.
(24) Roullier, V.; Grasset, F.; Boulmedais, F.; Artzner, F.; Cador, O.; Marchi-Artzner, V. *Chem. Mater*. **2008**, *20*, 6657–6665.
(25) Diana, F. S.; Lee, S. H.; Petroff, P. M.; Kramer, E. J. *Nano Lett*. **2003**, *3*, 891–895.
(26) Chen, M.; Liu, J. P.; Sun, S. *J. Am. Chem. Soc*. **2004**, *126*, 8394–8395.
(27) Glaria, A.; Kahn, M. L.; Falqui, A.; Lecante, P.; Colliere, V.; Respaud, M.; Chaudret, B. *ChemPhysChem* **2008**, *9*, 2035–2041.
(28) Castro, C.; Ramos, J.; Millan, A.; Gonzalez-Calbet, J.; Palacio, F. *Chem. Mater*. **2000**, *12*, 3681–3688.
(29) Korth, B. D.; Keng, P.; Shim, I.; Bowles, S. E.; Tang, C.; Kowalewski, T.; Nebesny, K. W.; Pyun, J. *J. Am. Chem. Soc*. **2006**, *128*, 6562–6563.
(30) Mikhaylova, M.; Berry, C. C.; Zagorodni, A.; Toprak, M.; Curtis, A. S. G.; Muhammed, M. *Chem. Mater*. **2004**, *16*, 2344–2354.
(31) Akcora, P.; Zhang, X.; Varughese, B.; Briber, R. M.; Kofinas, P. *Polymer* **2005**, *46*, 5194–5201.
(32) Belfield, K. D.; Zhang, L. *Chem. Mater*. **2006**, *18*, 5929–5936.
(33) Xia, H.; Foo, P.; Yi, J. *Chem. Mater*. **2009**, *21*, 2442.
(34) Xia, H.; Foo, P.; Yi, J. *Chem. Mater*. **2009**, *21*, 2442.
(35) Bielawski, C. W.; Grubbs, R. H. *Prog. Polym. Sci*. **2007**, *32*, 1–29.
(36) Marin, V.; Holder, E.; Hoogenboom, R.; Schubert, U. S. *Chem. Soc. Rev*. **2007**, *36*, 618–635.
(37) Kenneth John Ivin, J. C. M. *Olefin metathesis and metathesis polymerization*; Academic Press: New York, 1997; Chapter 11.
(38) Rodriguez-Escrich, S.; Popa, D.; Jimeno, C.; Vidal-Ferran, A.; Pericas, M. A. *Org. Lett*. **2005**, *7*, 3829–3832.
(39) Sasaki, H.; Haraguchi, Y.; Itotani, M.; Kuroda, H.; Hashizume, H.; Tomishige, T.; Kawasaki, M.; Matsumoto, M.; Komatsu, M.; Tsubouchi, H. *J. Med. Chem*. **2006**, *49*, 7854–7860.
(40) Wei, F.; Zhao, B. X.; Huang, B.; Zhang, L.; Sun, C. H.; Dong, W. L.; Shin, D. S.; Miao, J. Y. *Bioorg. Med. Chem. Lett*. **2006**, *16*, 6342–6347.
(41) Stamatov, S. D.; Stawinski, J. *Tetrahedron Lett*. **2007**, *48*, 1887–1889.
(42) Zhang, L.; Peritz, A.; Meggers, E. *J. Am. Chem. Soc*. **2005**, *127*, 4174–4175.

Scheme 1. Epoxy Monomer Synthesis

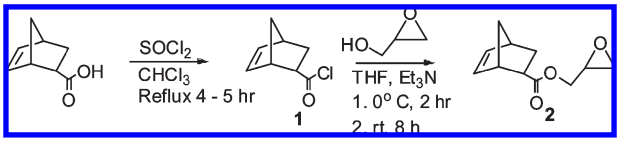

Experimental Section

Materials. Bicyclo[2.2.1]hept-5-ene 2-carboxylic acid (98% mixture of endo and exo), norbornene (99%), thionyl chloride (99.5%), glycidol (96%), triethylamine (99.5%), bis-(tricyclohexylphosphine)-benzylideneruthenium dichloride[43] (Grubbs' first generation catalyst, **3**), $Fe(CO)_5$ (99.9%), and trimethylamine *N*-oxide (98%), were purchased from Aldrich and used as received. CH_2Cl_2 and $CHCl_3$ were dried over $CaCl_2$ and distilled. THF was distilled over sodium and benzophenone under N_2 before use. Catalyst solutions were prepared in a glovebox.

Synthesis of Bicyclo[2.2.1]hept-5-ene-2-carboxylic Acid Oxiranylmethyl Ester (2). The synthetic procedure is illustrated in Scheme 1. The acid chloride was prepared by refluxing a mixture of *endo*- and *exo*-bicyclo[2.2.1]-hept-5-en-2-carboxylic acid (25.0 g, 0.204 mol) and thionyl chloride (30 mL, 0.408 mol) in dry $CHCl_3$ for 4−5 h under N_2.[44] The solvent was removed under reduced pressure, and the residue was purified by vacuum distillation at 0.5 torr at 42 °C, producing **1**, as a colorless liquid in 70% yield. Then, a mixture of triethylamine (22 mL, 0.16 mol) and glycidol (6.4 mL, 0.096 mol) was added over 2 h to the solution of the acid chloride (12 g, 0.08 mol) in dry THF at 0 °C. The mixture was then stirred at room temperature for 8 h. Et_2O was added and the resulting white salt was filtered off. The organic filtrate was washed with aqueous 5% NaOH solution, followed by washing with 5% HCl, saturated Na_2CO_3, and water. The solvent was removed under reduced pressure, and the residue was subjected to column chromatography (7:3 hexane: EtOAc on silica), affording **2** as a clear colorless oil (14.79 g, 95% yield). ^{1}H NMR (500 MHz, $CDCl_3$) δ: 6.06−6.14 (m, 1.5H, HC═C), 5.87 (m, 0.5H, HC═C), 4.10−4.39 (m, 1H, O—CH_2—CH), 3.78−3.89 (m, 1H, O—CH_2—CH), 3.16 (s, 1H), 2.78−2.99 (m, 3.5H), 2.58 (s, 1H, —CH—epoxy ring), 2.22 (m, 0.5H), 1.83−1.87 (m, 1H), 1.19−1.48 (m, 4H). ^{13}C NMR (125 MHz, $CDCl_3$) δ: 176.08, 174.58 (C═O exo and endo),138.28, 138.05 (C═C), 135.83, 132.46, 77.78, 77.35, 76.93, 65.17, 64.99, 64.90, 49.97, 49.96, 49.78, 47.01, 47.00, 46.66, 46.07, 44.98, 44.94, 43.52, 43.31, 42.86, 41.98, 30.77, 29.65, 29.61. IR (neat): 2974, 1734 (C═O strech), 1447, 1333, 1271, 1247 (C—O epoxide ring strech), 1232, 1171, 1064, 1031, 904, 847 cm^{-1}. Anal. calcd for $C_{11}H_{14}O_3$: C, 68.02; H, 7.27. Found: C, 67.89; H, 7.41.

Polymerization by ROMP of Bicyclo[2.2.1]hept-5-ene-2-carboxylic Acid Oxiranylmethyl Ester. ROMP of epoxy monomer **2** with Grubbs' first generation catalyst **3** was done according to a literature method and shown in Scheme 2. The catalyst solution was prepared by dissolving it[43] in anhydrous CH_2Cl_2 under N_2 atmosphere in a glovebox. The glassware was dried and purged with vacuum and N_2 in a Schlenk line several times prior to conducting the polymerization reaction.

(*a*) *Preparation of Homopolymer **4***. The epoxy monomer **2** (1.00 g, 5.15×10^{-3} M, 300 equiv) was dissolved in 35 mL dry CH_2Cl_2 and purged with N_2 gas. Then, an adequate volume of the catalyst solution (14 mg, 17.13×10^{-6} M, in 2 mL CH_2Cl_2, 1 equiv) was added to the reaction mixture and stirred for 4 h at 30 °C. The polymerization reaction mixture was terminated with ethyl vinyl ether (500 equiv relative to the catalyst) and stirred for another 1 h. Then, the reaction mixture was poured into cold methanol and stirred, purified, and dried under vacuum to give a flaky white solid (72% yield). ^{1}H NMR (500 MHz, $CDCl_3$) δ of 1:1 diblock copolymer: 5.12−5.24 (br, 2H, —HC═CH−), 4.30 (br, 1H), 3.82 (br, 1H), 3.09 (br, 1H), 2.34−2.90 (br, 2H), 0.85−1.70 (br).

(*b*) *Preparation of Diblock Copolymer **5***. The epoxy monomer **2** (1.15 g, 5.93×10^{-3} M, 200 equiv) was dissolved in 40 mL dry CH_2Cl_2 under N_2 gas. Then, the catalyst solution (25 mg, 30.38×10^{-6} M, in 2 mL CH_2Cl_2, 1 equiv) was added to the reaction mixture and stirred for 4 h at 30 °C. The pink color of the solution turned dark brown. The norbornene solution (0.55 g, 5.84×10^{-3}M in 40 mL CH_2Cl_2, 200 equiv) was injected and stirred for another 5 h. The polymerization reaction mixture was terminated with excess ethyl vinyl ether (500 equiv relative to the catalyst) and stirred for another 1 h. Then, the reaction mixture was poured into cold methanol and stirred, purified, and dried under vacuum to give flaky white solid in 92% yield. ^{1}H NMR (500 MHz, $CDCl_3$) δ of 1:1 diblock copolymer: 5.19−5.44 (br, 4H), 4.35 (br, 1H), 3.82 (br, 1H), 3.18 (br), 2.98, 2.64, 2.43, 1.97 (br), 0.85−1.70 (br).

Preparation of Stabilized Magnetic Nanoparticle Dispersions. Preparation of monodisperse maghemite nanoparticles within copolymer matrixes was accomplished by modification of known methods[45,46] as follows: the diblock copolymer was dissolved in cyclohexanone and heated to 100 °C, followed by addition of 0.2 mL of $Fe(CO)_5$ (1.52 mmol) under Ar. The mixture was refluxed for about 2 h until the yellow color of the solution turned black. It was then cooled to ambient temperature, and 0.34 g of trimethylamine *N*-oxide (4.56 mmol) was added to oxidize the iron nanoparticles. The mixture was refluxed for another 4 h, and the black dispersion of diblock copolymer-stabilized nanoparticles was observed. The dispersion was centrifuged, and the supernatant was collected. Ethanol was added to the supernatant, and black-brown precipitate was collected after further centrifugation. The black-brown precipitate was then redispersed in cyclohexanone or hexane. Two different formulations of maghemite−polymer nanocomposites were synthesized by varying the polymer weight (NC1-B1 3.3 wt % polymer; NC1-B2 0.97 wt % polymer) relative to a fixed amount of $Fe(CO)_5$ (0.2 mL) loading according to the procedure described above.

Characterization. ^{1}H NMR and ^{13}C NMR spectra were acquired on a Varian Mercury Gemini spectrometer at 500 and 125 MHz, respectively, using $CDCl_3$ as the solvent for all monomers and polymers. All FTIR studies were done using a Perkin-Elmer Spectrum One FTIR spectrometer from 4000 to 500 cm^{-1}. Thermogravimetric analysis (TGA) was performed with a TA Instruments model Q5000 TGA, from room temperature to 750 at 20 °C/min. All samples were dried under vacuum for 2 days before measurement. Differential scanning calorimetry (DSC) was conducted with a TA Instruments Q1000 DSC, from −10 to 250 °C at a rate of 10 °C/min. Transmission electron microscopy (TEM) was accomplished using a JEOL 1011 TEM, operated at 100 kV. A FEI Tecnai F30 TEM was used for ultrasmall nanocomposites. The samples were prepared

(43) Chuang, C.-J.; Li, W.-S.; Lai, C.-C.; Liu, Y.-H.; Peng, S.-M.; Chao, I.; Chiu, S.-H. *Org. Lett.* **2009**, *11*, 385–388.
(44) Biswas, S.; Belfield, K. D. *Polym. Prepr.* (*Am. Chem. Soc., Div. Polym. Chem.*) **2008**, *49*, 1063–1064.
(45) Hyeon, T.; Lee, S. S.; Park, J.; Chung, Y.; Na, H. B. *J. Am. Chem. Soc.* **2001**, *123*, 12798–12801.
(46) Euliss, L. E.; Grancharov, S. G.; O'Brien, S.; Deming, T. J.; Stucky, G. D.; Murray, C. B.; Held, G. A. *Nano Lett.* **2003**, *3*, 1489–1493.

Scheme 2. ROMP Block Copolymer Synthesis

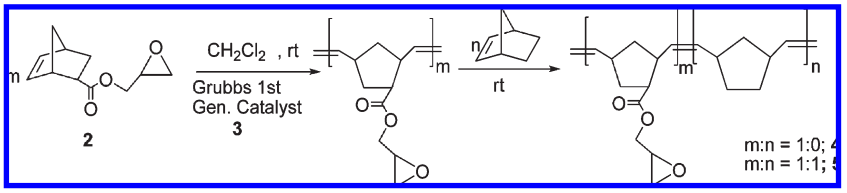

by evaporation of a dispersion of nanoparticles in the polymer on carbon-coated copper TEM grids. Selected area electron diffraction patterns were obtained in both cases. X-ray diffraction (XRD) (Geigerflex Rigaku2, $2\theta = 10 - 80°$, step = 0.05, dwell (s) = 3) was used to obtain powder X-ray diffraction pattern spectra using Cu Kα radiation (λ = 0.154 nm), and noise corrections were made by using MDI Jade 7 software. Gel permeation chromatography (GPC) was conducted with a Waters 2414 refractive index detector, Waters 2996 photodiode array, and Waters 1525 binary HPLC pump (THF as the mobile phase, flow rate of 1 mL/min) using Waters styragel HR2, HR5E columns and polystyrene as the standards.

Magnetic properties of the nanocomposites were measured using a superconducting quantum interference device (SQUID) magnetometer from Quantum Design. All the measurements were done in powder form of the sample after vacuum drying. The temperature dependence of the magnetization was determined by zero field-cooled (ZFC) and field-cooled (FC) measurements. The ZFC curve was obtained by cooling down to 5 K at zero magnetic fields and then measuring the magnetization under a 500 Oe applied magnetic field. The magnetization was measured during heating from 5 K to room temperature at 10 K intervals. The ZFC curve was obtained by cooling down to 2 K at zero fields and then measuring the magnetization under a 500 Oe applied magnetic field (for NC1-B1) up to 50 K. The corresponding FC curves were similarly obtained except that this time the sample was cooled while applying a 500 Oe magnetic field. The magnetizations as a function of applied magnetic field were also studied under constant temperature (below and above the blocking temperature).

Results and Discussion

Synthesis of Monomer 2. Monomer **2** was prepared according to Scheme 1. Acid chloride **1** was prepared in accordance to previous reports.[32] Norbornenyl oxiranemethyl ester **2** was prepared by the addition of a mixture of triethylamine and glycidol slowly with acid chloride **1**. After column chromatographic purification, a colorless oil was isolated in high yield. ^{1}H NMR analysis confirmed product formation by the appearance of new peaks at 4.39−3.78 ppm belonging to the proton adjacent to the ester, along with the characteristic vinyl peaks at 6.14−5.87 ppm for endo and exo monomers. Three new ^{13}C NMR peaks appeared at 65.17, 47.01, and 44.98 ppm. In addition, absorbances at 1247 and 1734 cm^{-1} in the FTIR spectrum corresponded to characteristic C—O stretching vibrations of the epoxy ring and C═O stretching vibrations of the ester, respectively.

Synthesis of Polymers 4 and 5. The homopolymer of epoxy monomer **2** and a diblock copolymer, containing anchoring and steric stabilizing blocks in ca. 1:1 molar ratio, were synthesized under mild conditions by ROMP, according to the procedure described in the Experimental Section (and shown in Scheme 2). Due to the air and water sensitivity of the Grubbs' catalyst, the catalyst solution was prepared in an anaerobic glovebox. Polymerization reactions were carried out using a Schlenk line under N_2. In order to prepare narrowly dispersed, well-defined block copolymers, the sequential order and time interval between addition of the different monomers is quite significant.[47] The extent of polymerization of monomer **2** was determined by ^{1}H NMR in $CDCl_3$. This study showed a new broad peak between 5.12 and 5.24 ppm, along with the gradual disappearance of the vinyl peaks of the monomer around 5.87−6.12 ppm, due to polymer formation. It took about 3.5 h for completion of the homopolymerization, i.e., complete monomer consumption (see the Supporting Information). In general, the propagation rate of the polymers depends on the polarity and stereochemistry (exo/endo) of the substituted ligand since the catalyst initiates polymerization from the exo side of the norbornene vinylic bond. The polymerization of unsubstiuted norbornene is more reactive relative to the norbornene substituted at the 2-position.[48,49] Hence, monomer **2** was used as the first block, followed by the addition of norbornene as the second block in the synthesis of diblock copolymer. A 1:1 block copolymer was chosen based on our previous study that indicated, among the different norbornene block copolymers, 1:1 block copolymers resulted in the best stabilization of maghemite nanoparticles.[32]

The molecular weight of the polymers was controlled by the monomer/initiator ([M]/[I]) feed ratio.[50] The monomer concentrations were kept at ca. 0.15 M in dry CH_2Cl_2, and polymerizations was performed at ca. 30 °C. Progression of the polymerization was followed by TLC (1:1 hexane:EtOAc). For block copolymer synthesis, after all the first block was consumed, the second monomer was added to the system. In general, the block copolymer required longer reaction time to yield blocks with narrow polydispersity compared to the homopolymer.

After all monomer was consumed, the polymerization was quenched by adding excess ethyl vinyl ether, with vigorous stirring, followed by precipitation in cold CH_3OH. The polymer was purified by redispersing in

(47) Ahmed, S. R.; Bullock, S. E.; Cresce, A. V.; Kofinas, P. *Polymer* **2003**, *44*, 4943–4948.
(48) Nishihara, Y.; Inoue, Y.; Nakayama, Y.; Shiono, T.; Takagi, K. *Macromolecules* **2006**, *39*, 7458–7460.
(49) Rule, J. D.; Moore, J. S. *Macromolecules* **2002**, *35*, 7878–7882.
(50) Zuercher, W. J.; Hashimoto, M.; Grubbs, R. H. *J. Am. Chem. Soc.* **1996**, *118*, 6634–6640.

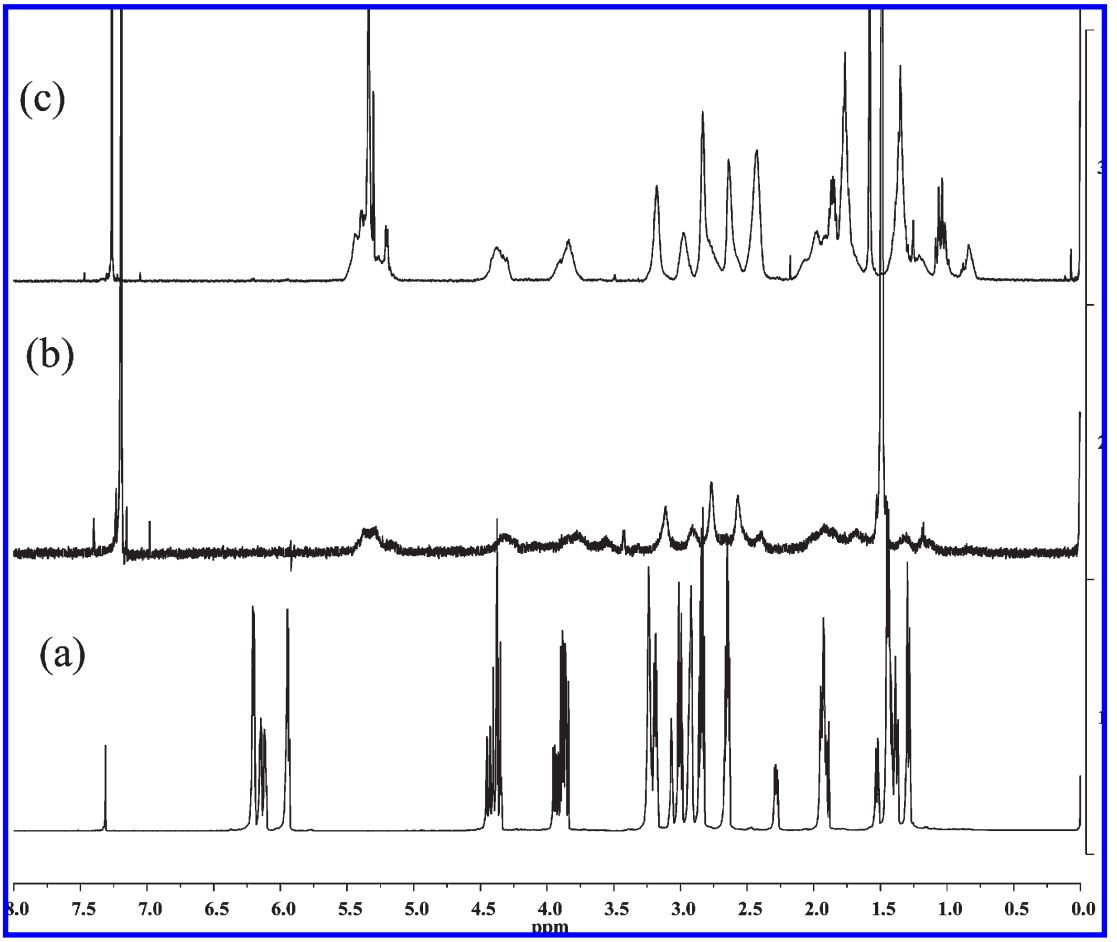

Figure 1. ^{1}H NMR of (a) monomer **2**, (b) homopolymer **4**, and (c) 1:1 block copolymer **3**.

Table 1. Polymer Characterization Data

block ratio (theo)	*m*:*n* (theo)	M_n[a] (theo)	*m*:*n* (^{1}H NMR)	M_n (GPC)	M_w (GPC)	PDI[b] (M_w/M_n)	block ratio[c] (calculated)	TGA[d] °C	T_g °C
300:0	1:0	58227	1:0	62391	69968	1.12	321:0	340	55
200: 200	1:1	57650	1:1	61464	88446	1.43	213:213	368	40

[a] Theoretical molecular weight calculated from [M]/[I] feed ratio. [b] M_n, M_w, and PDI were obtained from GPC in THF relative to polystyrene standards. [c] Actual polymer block ratio was calculated from the ^{1}H NMR and GPC results. [d] Temperature at 10% weight loss.

CH_2Cl_2 and reprecipitating in CH_3OH several times, followed by vacuum drying.

Characterization of Polymers 4 and 5. The structures of the polymers were confirmed by ^{1}H NMR analysis The vinyl protons of both norbornene and the epoxy ester monomer (5.87−6.12 ppm) gradually disappeared while new alkene resonances at 5.12−5.24 ppm appeared, ascribed to CH=CH protons in the polymer backbone (Figure 1). Each block ratio (*m*:*n*) was determined through integration of the proton NMR spectra. The new peaks at 5.12−5.24 ppm integrated to four protons and were contributed to from both blocks of the 1:1 copolymer backbone. The methylene peak from the epoxy block appeared at 4.30 (1H) and 3.82 (1H) ppm. The calculated and experimental block ratio (*m*:*n*) were in good agreement, substantiating the desired block lengths in the polymer backbone.

Molecular weights of the polymer were estimated via GPC analysis by using a universal calibration curve and polystyrene standards. The experimental molecular weight of the polymers was ca. 60 000 and polydispersity indexes (PDIs) were between 1.12 and 1.43 (Table 1). The narrow PDI, as well as the close agreement of the number average molecular weight of the polymers with the calculated molecular weight, is consistent with a well-controlled, living ROMP system.

Thermal properties of the polymers were evaluated by TGA and DSC, with results listed in Table 1. Homopolymer **4** started decomposing at nearly ca. 340 °C, slightly lower than the polynorbornene itself (ca. 400 °C),[51] while the 1:1 block copolymer (**3**) was stable up to 370 °C (thermograms are presented in the Supporting Information). The norbornene homopolymer and that with epoxy ester homopolymer **4** had a T_g of 31[52] and 55 °C, respectively. The 1:1 block copolymer (**4**) exhibited

(51) Janiak, C.; Lassahn, P. G. *Polym. Bull.* **2002**, *47*, 539–546.
(52) Dorkenoo, K. D.; Pfromm, P. H.; Rezac, M. E. *J. Polym. Sci., Part B: Polym. Phys* **1998**, *36*, 797–804.

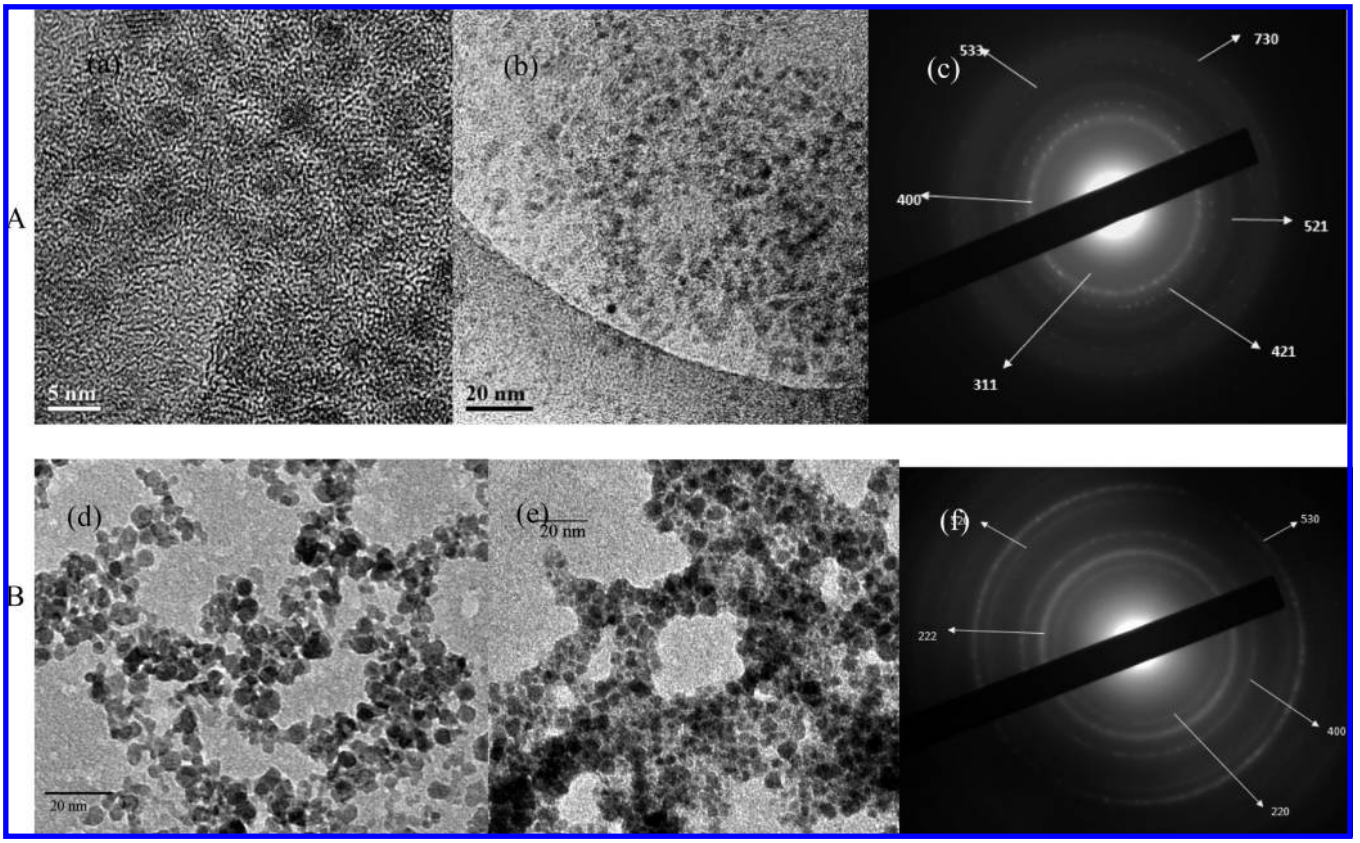

Figure 2. Transmission electron microscopy (TEM) images and electron diffraction pattern of (A) NC1-B1 and (B) NC1-B2.

a T_g of 40 °C, in good agreement with the theoretically predicted T_g value (40 °C) from the Fox equation.[53]

Synthesis of Maghemite−Block Copolymer Nanocomposites. The synthesis of polymer stabilized maghemite nanopaticle dispersions provided uniform, monodisperse, highly crystalline nanocrystallites. Stabilized γ-Fe_2O_3 nanoparticle ferrofluids were prepared with the 1:1 norbornene diblock copolymer in cyclohexanone by an in situ process. Maghemite−block copolymer nanocomposites were prepared using the 1:1 block copolymer as surfactant in cyclohexanone, via thermal decomposition of $Fe(CO)_5$, followed by oxidation with trimethylamine oxide. The 1:1 block copolymer was used for the nanocomposite preparation and its study, as we preiously established that 1:1 balance between the chelating block and the steric stabilizing block in a norbornene-based copolymer results in good magnetic nanoparticle stabilization. Two different formulations were prepared by varying the weight percent of 1:1 diblock copolymer (NC1-B1 3.3 wt %; NC1-B2 0.97 wt %) relative to a constant volume of $FeCO_5$ feed, to evaluate this effect on the formation of nanoparticles, its morphology, and the magnetic properties of the nanocomposite.

Characterization of Maghemite−Block Copolymer Nanocomposite. TEM, X-ray diffraction, and FTIR were used to obtain information about the maghemite nanoparticles dispersed in the polymer matrix.

Morphology and Particle Size. TEM analysis confirmed the generation of well-controlled uniform and spherical iron oxide nanoparticles, encapsulated by the self-assembled block copolymers. Interestingly, depending on the weight percent of polymer loading, and thus the relative amount of chelating and steric stabilizing groups present in the polymer, the size of the nanoparticles can be controlled. The nanocomposite NC1-B1, with high polymer loading, resulted in smaller nanoparticles with 2−3 nm average diameters, while the nanocomposite NC1-B2 generated nanoparticles with an average diameter of 5−6 nm (Figure 2). In both cases, the 1:1 block copolymer was able to stabilize maghemite nanoparticles quite efficiently without any noticeable aggregation.

In addition, selected area electron diffraction patterns (see Supporting Information) were obtained for both of the nanocomposites in order to examine the crystalline structure present in the nanocomposite (Figure 2c and f). Electron diffraction patterns of the nanoparticles were consistent with the standard crystal structure and *d* spacing of γ-Fe_2O_3.

Crystalline Phase. The X-ray diffraction pattern (Figure 3B) of NC1-B2 was in good agreement with the standard γ-Fe_2O_3 reflection [PDF no. 00-039-1346; Maghemite-C, syn; cubic], confirming the nanoparticles formed were Fe_2O_3. The Fe_2O_3 nanoparticles displayed several strong reflection peaks in the 2θ region of 20−70°. The strong Bragg reflections of Fe_2O_3 are at the 2θ angles of 30.24° (d = 2.95°A), 35.35° (d = 2.51°A), 43.15° (d = 2.09°A), 56.80° (d = 1.64°A), and 62.70° (d = 1.48°A).

(53) Pochan, J. M.; Beatty, C. L.; Pochan, D. F. *Polymer* **1979**, *20*, 879–886.

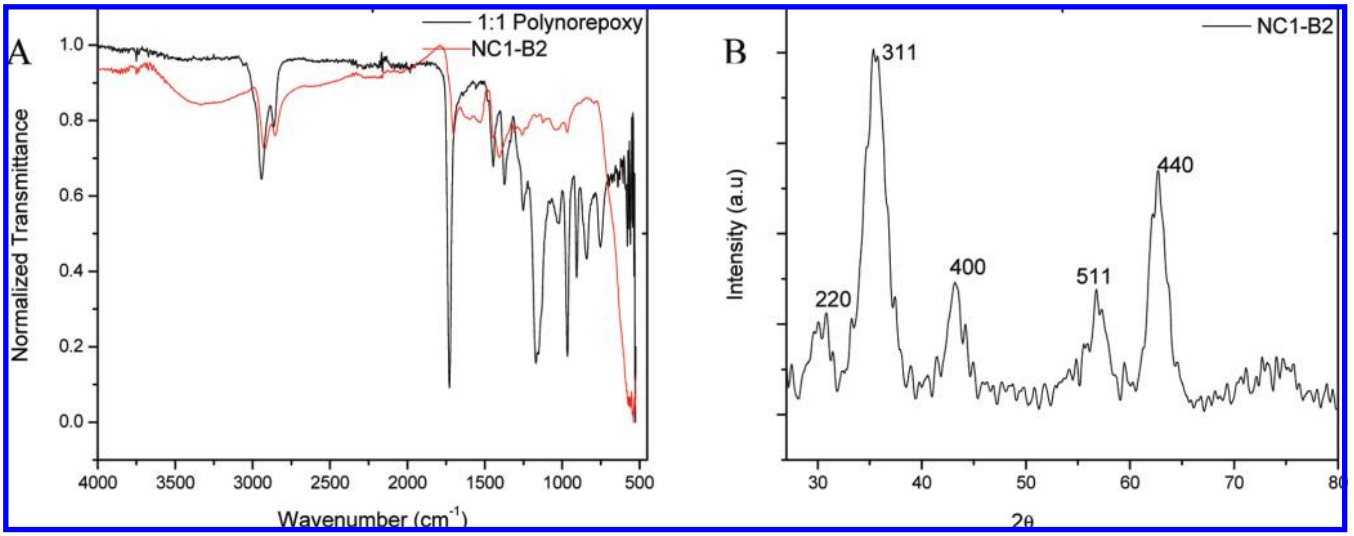

Figure 3. FTIR analysis for (A) γ-Fe_2O_3 nanoparticles stabilized by block copolymer **3** and 1:1 block copolymer **3** alone. (B) XRD pattern for γ-Fe_2O_3 nanoparticles stabilized by block copolymer **3** (NC1-B2) in powder form.

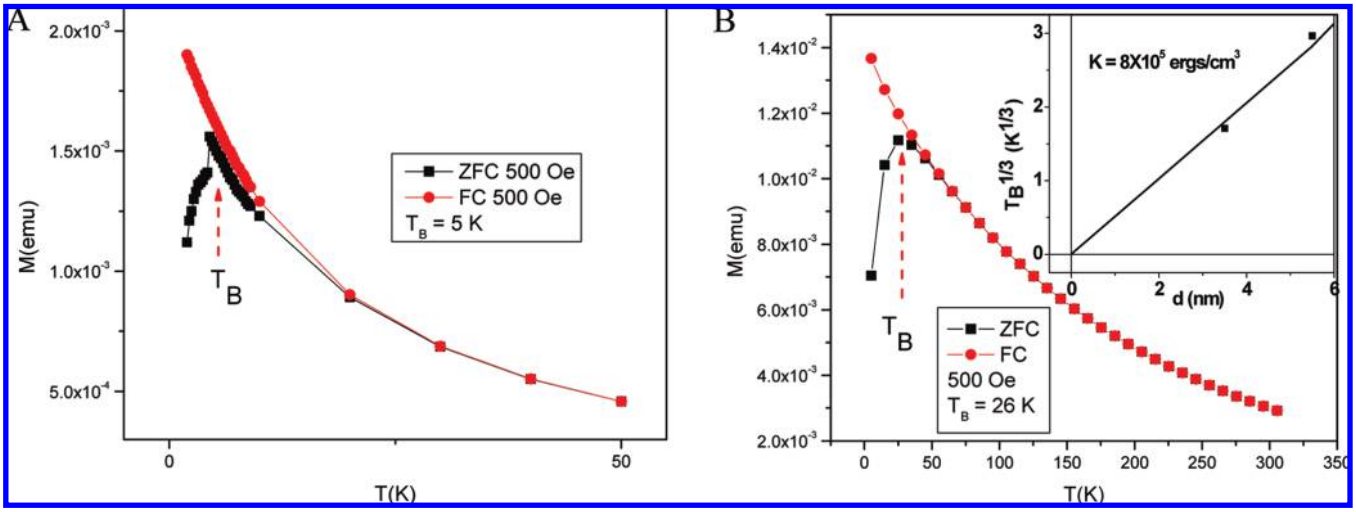

Figure 4. Magnetization (M) as a function of temperature (T) at 500 Oe applied magnetic field, for (A) NC1-B1 and (B) NC1-B2. (b inset) Linear behavior of $T^{1/3}$ as a function of particle diameter (d) through the origin.

These corresponded to the indices (220), (311), (400), (511), and (440), respectively. The average diameters (d) of the singular γ-Fe_2O_3 nanocrystallites were estimated using Scherrer equation.[34] The estimated d value associated with the strongest (311) reflection of the Fe_2O_3 at 2θ 35.35° was about 6 ± 1 nm, which was in good agreement with the average size of singular nanoparticles observed from TEM. However, the XRD analysis of NC1-B1 was unable to extract sufficient distinct peaks due to the ultrasmall particle size of the maghemite nanocrystals. For very small nanocrysalites, this fact is supported by previous reports,[27] although from the electron diffraction pattern in the TEM experiment the presence of γ-Fe_2O_3 was confirmed.

Maghemite−Polymer Chemical Binding. FTIR spectroscopy was quite informative in characterization of the block copolymer as well as the nanocomposite, suggesting complexation of the iron oxide nanoparticles and the pendant epoxy of the block copolymer, thereby rendering the iron oxide particles noninteracting. There was a distinct difference in the FTIR spectrum (Figure 3A) of the maghemite−polymer nanocomposite with respect to the polymer alone. In the nanocomposite, a single, broad band due to the Fe—O stretch at ca. 580 nm was present and is characteristic of γ-Fe_2O_3 particles less than 8 nm.[54] A broad peak was observed at ca. 3350 cm^{-1} in the polymer−maghemite nanocomposite, possibly due to OH stretching as a result of opening of the epoxy ring. Furthermore, the C═O stretching vibration shifted from 1729 cm^{-1} in the polymer to 1692 cm^{-1} in the nanocomposite, indicative of interaction between the

Table 2. Summary of Magnetic Properties of the Maghemite−Block Copolymer Nanocomposites

nanocomposite	wt % polymer loading	average particle size (nm)	T_B (K)	M_s (emu/g)
NC1-B1	3.3	3.5	5	63 at 50 K
NC1-B2	0.97	5.5	26	64 at 100 K

(54) Li, D.; Teoh, W. Y.; Selomulya, C.; Woodward, R. C.; Munroe, P.; Amal, R. *J. Mater. Chem.* **2007**, *17*, 4876–4884.

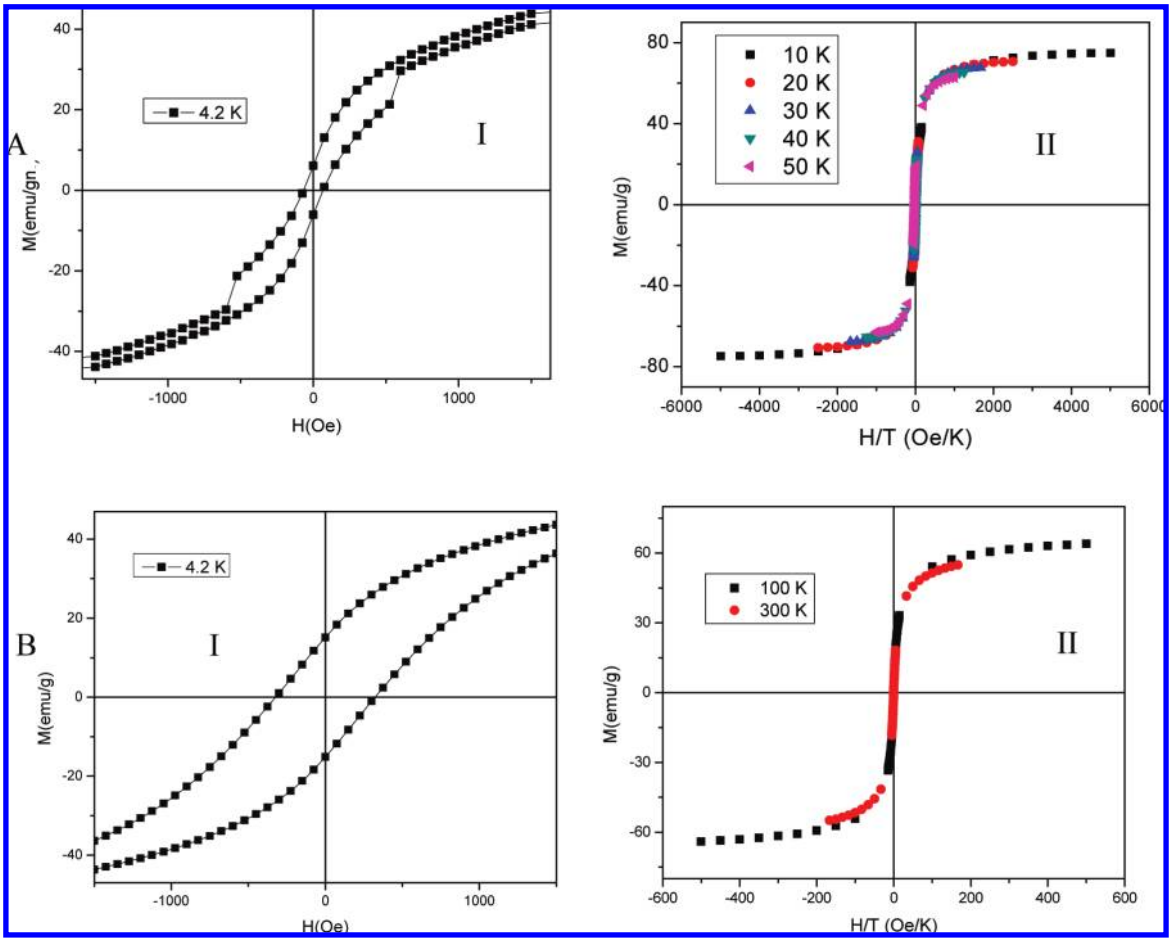

Figure 5. Magnetization (M) versus applied magnetic field (H) at constant temperature for (A) NC1-B1 and (B) NC1-B2. In each case, I shows hysteresis below the blocking temperature and II shows no hysteresis above the blocking temperature with H/T scaling as expected for superparamagnetic particles.

metal core and the chelating block of the polymer. The coordination assembly of polymer to the iron-oxide core is believed to contain stable ring structures which assist in stabilizing the nanoparticles. This chelation is consistent with opening of the strained epoxy ring to generate free OH groups.

Magnetic Properties. Magnetic measurements were performed on both of the γ-Fe_2O_3−polymer nanocomposites (NC1-B1 and NC1-B2) in powder form using a Quantum Design superconducting quantum interference device (SQUID). Both nanocomposites exhibited behavior typical of noninteracting ferromagnetic nanoparticles with uniform size. The temperature dependent magnetizations $M(T)$ for both field-cooled (FC) and zero-field-cooled (ZFC) cases are shown for the samples NC1-B1 and NC1-B2 in Figure 4A and B, respectively. The peak in the ZFC magnetization corresponds to the blocking temperature (T_B), shown by vertical dotted red arrows. The values of T_B for the samples NC1-B1 and NC1-B2 are 5 and 26 K, respectively. The values are also listed in Table 2. The higher value of T_B for the NC1-B2 compared to NC1-B1 is consistent with the fact that NC1-B2 has larger particle size (5.5 nm diameter) than NC1-B1 (3.5 nm diameter). The cube root of the ratio of $T_{B(B2)}$ to $T_{B(B1)}$ is 1.7, and the ratio of the respective diameters is 1.6. The close agreement of these ratios suggests that T_B grows linearly with the volume of the particle as expressed by the equation[55]

$$T_B = KV/k_B \ln(\tau_m/\tau_0) \quad (1)$$

where K is the crystalline anisotropy constant, k_B is the Boltzmann constant, V is the volume of the particle, τ_m is the measurement time (typically 100 s), and τ_0 is the inverse of the attempt frequency associated with magnetic moments overcoming field-dependent energy barriers. The inset of Figure 4B shows the dependence of $T_B^{1/3}$ on the particle diameter d for the two samples with the linear fit (solid line) forced through the origin. This good agreement with eq 1 allows us to calculate $K = 8 \times 10^5$ ergs/cm^3 where we have set $\ln(\tau_m/\tau_0)$ to be on the order of 25, as is commonly done in this type of calculation.[56] This value for K is in good agreement with the previous observations on the same material.[57]

Magnetization loops are shown in Figure 5A and B at the indicated temperatures for the samples NC1-B1 and NC1-B2, respectively. Figure 5A I (5B I) shows the magnetization loop at 4.2 K for NC1-B1 (NC1-B2). Both

(55) Stoner, E. C.; Wohlfarth, E. P. *Phil. Trans. R. Soc. A* **1948**, *240*, 599–642.
(56) Skomski, R. *J. Phys.: Condens. Matter* **2003**, *15*, R841–R896.
(57) Coey, J. M. D. *Phys. Rev. Lett.* **1971**, *27*, 1140.

Figure 6. Photographs of (A) γ-Fe_2O_3 nanoparticles stabilized by 1:1 block copolymer NC1-B2 in cyclohexanone and (B) the same ferrofluid under the influence of external magnetic field.

of the loops show hysteretic behavior as expected below T_B. The coercive field H_c determined from the loop is 60 Oe (340 Oe) for NC1-B1 (NC1-B2). Since H_c increases with increasing particle size, the particles are likely to be single domain and coherently rotating.[58,59] The temperature dependence of H_c for coherently rotating single domain particles with random orientations of the easy axis of magnetization is given by the relation[60]

$$H_c = \frac{2K}{M_s}\left[1-\left(\frac{T}{T_B}\right)^{3/4}\right] \qquad (2)$$

where M_s is the saturation magnetization. Both K and M_s are intrinsic quantities independent of particle size. Using eq 2, the ratio H_{cB2}:$H_{cB1} \sim 6$ is calculated at $T = 4.2$ K. The ratio of the H_c's determined from the respective magnetization loops is (340/60) 5.7. This good agreement suggests that the particles are in fact uniform in size, noninteracting, single domain, and coherently rotating with the easy axis of the magnetization randomly oriented.

As expected, the magnetization loops for $T > T_B$ are shown in Figure 5A II (5B II) for the sample NC1-B1 (NC1-B2) and do not show hysteresis, i.e., $H_c = 0$. Note the H/T scale on the x axis. All the loops at different temperatures fall on top of each other. This type of scaling is the signature of noninteracting superparamagnetic particles.[61]

The results from the magnetic measurements are listed in Table 2. The magnetization loop above the blocking temperature is fit with the Langevin function. The saturation magnetization M_s is approximately 60 emu/g as determined from the fit. This is consistent with the previous observation.[62,63] Figure 6A shows the 1:1 block copolymer-stabilized (NC1-B2) maghemite nanoparticle dispersion in cyclohexanone at room temperature. Figure 6B shows the effect of an external magnetic field on the same ferrofluid, further demonstrating the magnetic properties of the system.

Conclusions

In this work, we have demonstrated the synthesis and characterization of novel norbornene backbone-based well-defined block copolymers, containing both a steric stabilizing segment and an epoxy ester chelating group via ROMP. The molar ratio between these two blocks was determined to be 1:1 by ^{1}H NMR study while the molecular weight was estimated from GPC analysis. The thermal properties of the polymer demonstrated that the polymers possesses good thermal stability up to 360 °C with glass transition temperature of 40 °C, in good agreement with that calculated with the Fox equation and the T_g of the two corresponding homopolymers. Well-contolled, monodisperse iron-oxide nanoparticles were synthesized in the presence of the 1:1 diblock polymer matrix with two different polymer loadings, resulting in uniform spherical nanocrystallites with an average diameter between 2 and 6 nm, depending on the amount of block copolymer present.

The morphology, chemical nature, and the crystalline structures of the maghemite−polymer nanocomposites were evaluated with TEM, FTIR, and XRD analysis, respectively. The stabilized maghemite−polymer nanocomposites had a monodisperse nanoparticle morphology, with a lattice structure resembling the maghemite−C-syn structure. FTIR analysis supports coordination assembly of the polymer to the iron-oxide core, likely containing stable ring structures that assist in stabilizing the nanoparticles. This chelation is consistent with opening of the strained epoxy ring to generate free OH groups. The coordination between epoxy ester groups with the iron oxide nanoparticles prevent maghemite nanopatricle agglomeration and generated stabilized magnetic nanocomposites.

The magnetic properties of the nanocomposites were measured in dry powder form using a SQUID magnetometer, demonstrating the superparamagnetic nature of the nanocomposites at room temperature. The dc magnetization versus temperature ZFC curve indicated low blocking temperatures of ca. 5 K for one polymer nanocomposite containing smaller particles and 26 K for the composite consisting of slightly larger particles. Our measurements of magnetic properties indicate the presence of single domain maghemite nanoparticles in the nanocomposite in which the 1:1 block copolymers were able to mask the nanoparticles efficiently by chelation through epoxy and ester groups. Both of the nanocomposites exhibited very small hysteresis below the blocking temperature and no hysteresis above this temperature, characteristic of superparamagnetism. Finally, the magnetization vs applied magnetic field showed very high saturation magnetization values of ca. 60 emu/g for the magnetic polymer nanocomposites. Thus, the magnetization data

(58) Kneller, E. F.; Luborsky, F. E. *J. Appl. Phys.* **1963**, *34*, 656.
(59) Das, R.; Gupta, A.; Kumar, D.; Hoh, S.; Pennycook, S. J.; Hebard, A. F. *J. Phys.: Condens. Matter* **2008**, *20*, 5.
(60) Garcia-Otero, J.; Garcia-Bastida, A. J.; Rivas, J. *J. Magn. Magn. Mater.* **1998**, *189*, 377–383.
(61) Mao, Z. Q.; Chen, D. H.; He, Z. H. *J. Magn. Magn. Mater.* **2008**, *320*, 2335–2338.
(62) Dutta, P.; Manivannan, A.; Seehra, M. S.; Shah, N.; Huffman, G. P. *Phys. Rev. B* **2004**, *70*, 7.
(63) Pascal, C.; Pascal, J. L.; Favier, F.; Moubtassim, M. L. E.; Payen, C. *Chem. Mater.* **1999**, *11*, 141–147.

strongly suggest that the particles synthesized and stabilized by well-defined block copolymers, as described in this paper, are stable, noninteracting, single domain, coherently rotating, and uniform in size nanocomposites.

Acknowledgment. We wish to acknowledge the National Science Foundation (ECS-0103587, CHE-0832622, and DMR-0704240) for support of this work.

Supporting Information Available: .Monitoring the course of polymerization of the norbornylepoxy homopolymer via ^{1}H NMR (Figure S1), GPC results of polymers (Figure S2), TGA and DSC thermograms of the polymers (Figure S3), electron diffraction patterns (Figures S4 and S5) of the nanocomposites from TEM along with comparison with the standard maghemite nanocrystals are presented. This material is available free of charge via the Internet at http://pubs.acs.org.